Multifractal analysis of ^{197}Au-emulsion collisions at 10.6A GeV

G. Singh and P. L. Jain
High Energy Experimental Laboratory, Department of Physics,
State University of New York at Buffalo, Buffalo, New York 14260
(Received 18 March 1994)

We compute the multifractal moments G_q in terms of a new scaled variable X suggested by Bialas and Gazdzicki to study the dynamical fluctuations of particles produced in the interactions of ^{197}Au at 10.6A GeV with nuclear emulsion. An asymptotic power-law dependence of the moments on the bin size δX has been observed in pseudorapidity (η), azimuthal (ϕ), and η-ϕ phase spaces. The dynamical values of the generalized dimensions are determined in all the phase spaces. The dynamical properties of the produced particles are mapped onto smooth multifractal spectra $f(\Delta\alpha_q)$ by excluding the statistical contribution. The ^{197}Au results are compared with a ^{28}Si ion at 14.5A GeV and a ^{32}S beam at 200A GeV.

PACS number(s): 25.75.+r

I. INTRODUCTION

Bialas and Peschanski [1] suggested the method of scaled factorial moments in order to find out the origin of nonstatistical fluctuations in the distributions of the secondary particles produced in high energy collisions. Such fluctuations reveal the self-similar behavior of multiplicity fluctuations in particle production at high energy. The nonstatistical particle density fluctuations in high energy collisions have been observed in several experiments [2], when the scaled factorial moments F_q [1] are studied as a function of the phase space interval size down to the limit of the detector resolution. The conjectured power-law behavior of the scaled factorial moments [1] is known as intermittency in analogy with the description of bursts of turbulence in the theory of chaos. The intermittent behavior appears to be a general property of particle production at relativistic energies [2].

Analogous to the well-known phenomenon of self-similarity in geometrical and statistical systems, it has been suggested that the multiparticle production data may also exhibit fractal behavior [3]. The power-law behavior of the scaled F_q moments, indeed, implies the existence of some kind of fractal patterns [4,5] in the dynamics of the particles produced in their final state. Therefore, it is natural to address the concept of self-similarity under the perspective of fractal properties of the hadronic matter in multiparticle production. A formalism to investigate quantitatively any single particle density distribution in the framework of multifractal characteristics has been recently proposed [5], and it involves the computation of multifractal moments, G_q, as a function of the phase space intervals. The technique of multifractal moments has been recently applied successfully to understand the self-similarity of the hadronization mechanism prevailing in leptonic [6], hadronic [7], and nuclear collisions [8] at relativistic energies.

We presented experimental evidence on the existence of multifractal properties of singly charged hadrons emerged in nucleus-nucleus collisions over a wide range of energies [8,9], and, subsequently, of the projectile fragments of charge $Z \geq 2$ produced at energies $< 2A$ GeV [10]. So far, no data are available on the analysis of multifractal structures of the produced hadrons at the Brookhaven Alternating Gradient Synchrotron (AGS) energy with a projectile of mass more than the ^{28}Si beam. Very recently, a massive ^{197}Au projectile was accelerated to an energy of 10.6A GeV from the AGS at Brookhaven National Laboratory (BNL). Our aim is to explore the multifractal properties in the currently collected data on ^{197}Au-emulsion collisions in the pseudorapidity (η), azimuthal (ϕ), and η-ϕ phase spaces using a new scaled variable X suggested by Bialas and Gazdzicki [11]. We shall then compare the results of ^{197}Au beam with two additional data samples: (i) 14.5A GeV ^{28}Si beam [12] obtained from BNL and (ii) 200A GeV ^{32}S ion [13] obtained from CERN, an ion with the highest available energy per nucleon.

II. EXPERIMENTAL TECHNIQUE

The data presented here were obtained by irradiating the Fuji emulsion pellicles to a beam of ^{197}Au ions at 10.6A GeV (projectile) A) from Brookhaven National Laboratory (Expt. No. 875). The details of scanning and angular measurement techniques are discussed elsewhere [14,15]. For angular measurements, we selected a sample of 245 ^{197}Au events such that the projectile fragments of charges $1 \leq Z \leq 17$ survived in an interaction, and also the number of singly charged produced shower particles (N_s) in a collision was always > 50, with the number of low energy target tracks, $N_h \geq 0$. The produced shower particles N_s are predominantly relativistic pions with velocity $\beta = v/c > 0.7$. N_h represents the number of low energy ($\beta \leq 0.7$) heavy particles emerged from the target nucleus of emulsion [15]. While performing the angular measurements, utmost care was taken to exclude uninteresting background shower tracks emerging from pion-gamma conversion to e^+e^- pairs. These

shower tracks almost occur in the same plane in emulsion and when followed downstream showed a considerable amount of Coulomb scattering. An experienced observer, while doing the angular measurements, can easily catch them and exclude them. In addition to it, another source of unwanted background due to double counting of the shower tracks was also avoided. By using the reference primary method [15], we achieved an accuracy of 0.1 mrad in measuring the emission angles (θ) of shower particles in the central pseudorapidity region ($\eta = -\ln\tan\theta/2$). We compared the ^{197}Au beam (projectile A) results with the 14.5A GeV ^{28}Si ion (projectile B) from BNL (Expt. No. 847) and with the 200A GeV ^{32}S nucleus (projectile C) from CERN (Expt. No. EMU08). For B and C data sets, we selected only the events with complete destruction of the beam nucleus into singly charged projectile fragments. The numbers of events used for projectiles B and C were 172 and 200, respectively. The analysis was confined to the pionization region in each case. The selected ranges of pseudorapidity intervals were $\Delta\eta$ =0.5–3.7, 0.5–3.9, and 0.4–6.4 for projectiles A, B, and C, respectively. The average multiplicities of the singly charged particles $\langle N_s\rangle$ in the investigated $\Delta\eta$ ranges are 139.5 ± 11.5, 62.6 ± 4.8, and 207.4 ± 14.7 for the ions A, B, and C, respectively. For azimuthal ϕ phase space, the analysis was performed on the shower particles falling in the above-mentioned $\Delta\eta$ range of an individual projectile.

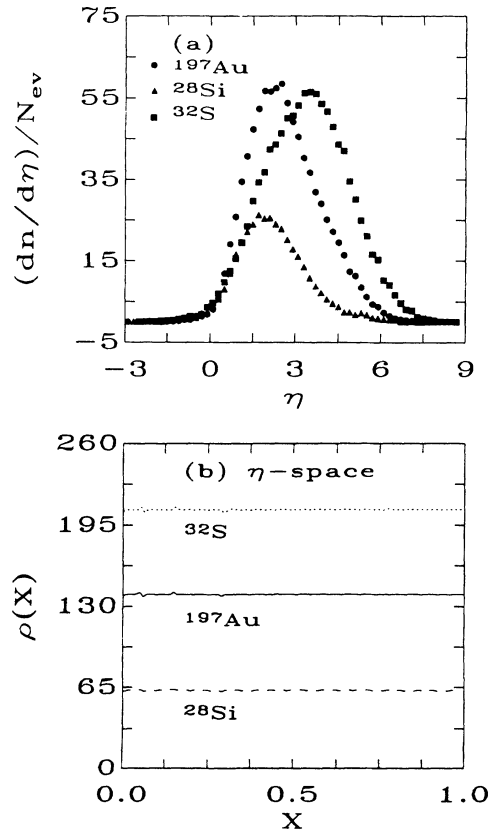

FIG. 1. (a) Single particle pseudorapidity distributions $\rho(\eta)$ for the projectiles A, B, and C. (b) Single particle density distributions $\rho(X)$ of the scaled variable $X(\eta)$ for the above ions.

In Fig. 1(a), we show the singly charged particle pseudorapidity densities $\rho(\eta)$ for the three projectiles A, B, and C used. One may notice that the $\rho(\eta)$ distribution is not completely uniform over the investigated $\Delta\eta$ range in each case. Each of the distributions suffers from edge effects and hence may not be suitable to investigate the multifractal moments G_q. Since G_q moments depend on the shape of the single particle density distribution, it is advisable to circumvent the problem of edge effects. To avoid it and also to compare the results obtained from several experiments, where the basic observables are different, Bialas and Gadzicki [11] have suggested a new scaled variable X related to the single particle density distribution $\rho(\eta)$ as

$$X(\eta) = \int_{\eta 1}^{\eta} \rho(\eta)d\eta \Big/ \int_{\eta 1}^{\eta 2} \rho(\eta)d\eta \ . \tag{1}$$

Here, η_1 and η_2 are the two extreme limits of the pseudorapidity distribution. For a given value of the pseudorapidity η falling in the interval $\Delta\eta = \eta_2 - \eta_1$ of an individual shower track in an event, the X variable was created using Eq. (1). The variable X varies uniformly between 0.0 and 1.0, so that $\rho(X) \approx$ constant with η_1 and η_2 as depicted in Fig. 1(b) for the projectiles A, B, and C in η phase space. The value of $\rho(X)$ as expected is the highest for the ^{32}S projectile and the lowest for the ^{28}Si projectile. For ^{197}Au, it lies almost at the middle of the distributions for ^{32}S and ^{28}Si beams. Similar results were also obtained for the $X(\phi)$ and $X(\eta\phi)$ variables (not shown here). The present analysis, therefore, deals with the computation of G_q moments from the single particle $X(\eta)$, $X(\phi)$, and $X(\eta\phi)$ density distributions, instead of the usual pseudorapidity η, azimuthal ϕ, and η-ϕ distributions.

III. THEORETICAL FORMALISM

According to the theory of multifractals [5], N singly charged shower particles falling in a given interval $\Delta X = X_{\max} - X_{\min}$ are distributed into M nonempty bins with a bin size $\delta X = \Delta X/M$. The power-law dependence of $\langle G_q\rangle$ of order q on X for the self-similar fluctuations, when $N/M \gg q$, is expressed as

$$\langle G_q\rangle = \frac{1}{N_{\rm ev}} \sum_{1}^{N_{\rm ev}} \sum_{j=1}^{M} (n_j/N)^q \propto \delta X^{-\tau_q}, \tag{2}$$

where n_j denotes the multiplicity of charged particles detected in the jth bin and $N = \sum_{j=1}^{M} n_j$ denotes the total number of particles detected in an event. The exponents q extend over all real numbers. $N_{\rm ev}$ stands for an ensemble of events analyzed in a given data set. τ_q are the generalized exponents and can be determined unambiguously from the asymptotic behavior. A linear dependence of $\langle \ln G_q\rangle$ on $-\ln\delta X$ over all the windows is related to $\tau_q = \lim_{\delta X\to 0}(\Delta\langle \ln G_q\rangle/\Delta \ln \delta X)$. From the derivatives

of τ_q, α_q is determined and by the Legendre transformations, one obtains the spectral function $f(\alpha_q)$ as follows:

$$\alpha_q = \frac{d\tau_q}{dq}, f(\alpha_q) = q\alpha_q - \tau_q \ . \tag{3}$$

For the presence of multifractal structures in a particular data sample, the spectral function $f(\alpha_q)$ must have (i) downward concave form, (ii) $f(\alpha_q)$ has a maximum value at $\alpha_q = \alpha_0$, and (iii) $f(\alpha_q) < f(\alpha_0)$, for $q \neq 0$. The width of the $f(\alpha_q)$ distribution is a measure of the size of dynamical fluctuations. For a purely statistical system with absolutely no fluctuations, $f(\alpha_q) = \alpha_q = 1$ for all values of q and the function $f(\alpha_q)$ is a straight line parallel to the y axis at $\alpha_q = 1$. The generalized dimensions D_q [4,5] of the multifractals are related to the mass exponents τ_q by

$$D_q = \frac{\tau_q}{q-1} \ , \tag{4}$$

for $q \neq 1$. Here, $D_0 = f(\alpha_0)$, $D_1 = f(\alpha_1) = \alpha_1$, and $D_2 = 2\alpha_2 - f(\alpha_2)$ are known as the fractal, information, and correlation dimensions, respectively.

IV. RESULTS AND DISCUSSION

In Fig. 2(a), we plot a variation of $\langle \ln G_q \rangle$ as a function of $-\ln \delta X$ for projectile A in η phase space. Clearly, a linear dependence of $\langle \ln G_q \rangle$ on $-\ln \delta X$ is demonstrated (except for a few last data points for $q = -6$ and $q = -7$), which is a qualitative measure of the manifestation of the multifractal structures exhibited by the ^{197}Au-emulsion reactions at BNL. To compare the results, similar plots are shown for projectiles B and C in Figs. 2(b) and 2(c), respectively. The multifractal characteristics are also observed for the projectiles B and C. The errors quoted in Figs. 2(a)–2(c) are calculated on the basis of the total number of shower particles falling in each bin. For the negative values of q, ^{28}Si data at 14.5A GeV show saturation effects much earlier as compared to ^{197}Au and ^{32}S data sets. This is due to the fact that the mean multiplicity of shower particles $\langle N_s \rangle$ for ^{28}Si data is much less in comparison to the other two data samples. As the bin width δX is decreased, more and more nonempty bins contain only one shower particle and the scaling properties of the G_q moments are lost for the bins containing only a single particle. Thus, the multifractal structures can be observed only if more shower particles are available in each bin and when the saturation starts; we do not consider those bins for linear relation. However, for the positive values of q, the saturation effect seems to be almost nonexistent for all the beams A, B, and C.

It is interesting to examine the multifractality in the dynamics of produced singly charged particles in the azimuthal ϕ phase space also. To achieve this objective, the above analysis is repeated over the X variable in azimuthal plane. The outcome of such a study is presented in Figs. 3(a), 3(b), and 3(c) for the projectiles A, B, and C, respectively. Except for a few last data points, a linear of $\langle \ln G_q \rangle$ with $-\ln \delta X$ is observed for all the data sets.

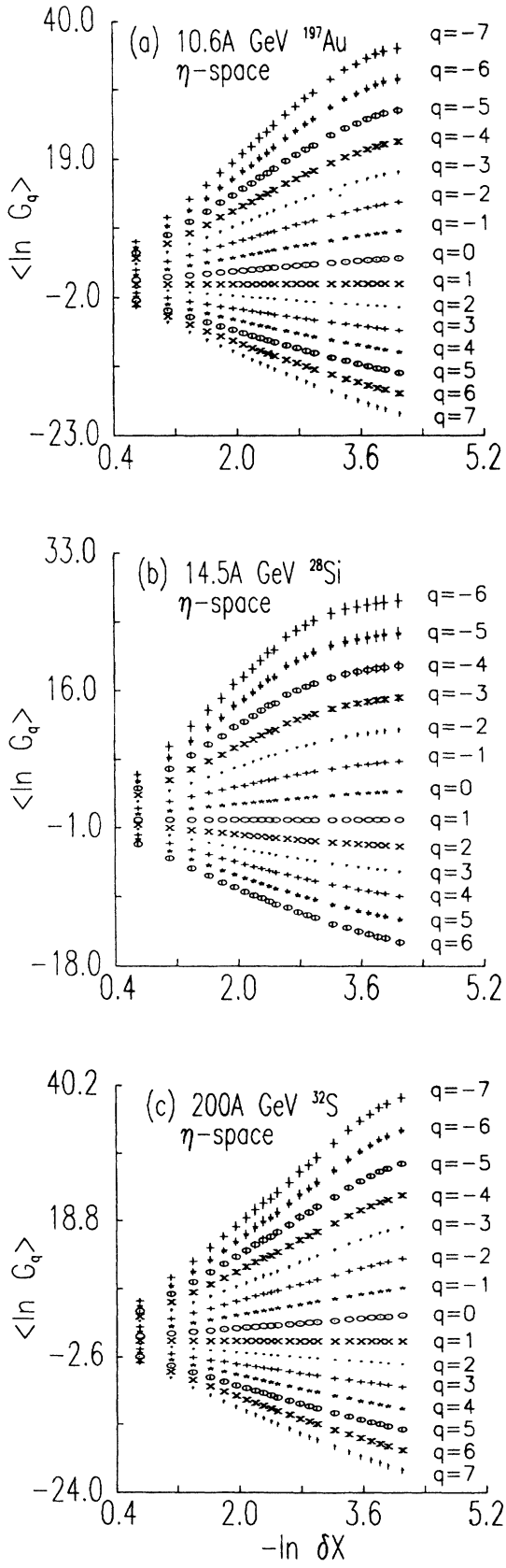

FIG. 2. $\langle \ln G_q \rangle$ as a function of $-\ln \delta X$ for (a) ^{197}Au at 10.6A GeV, (b) ^{28}Si at 14.5A GeV, and (c) ^{32}S at 200A GeV in η phase space.

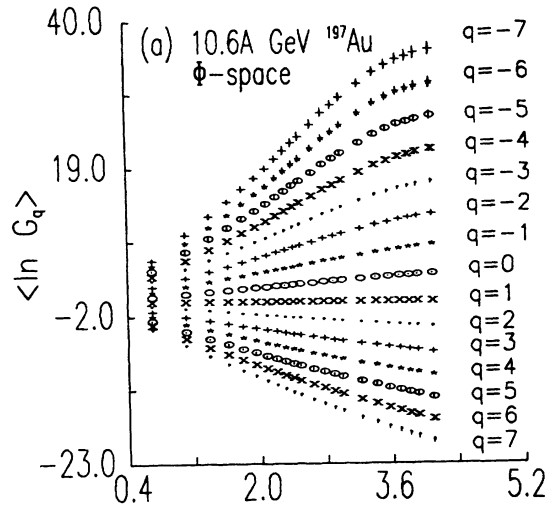

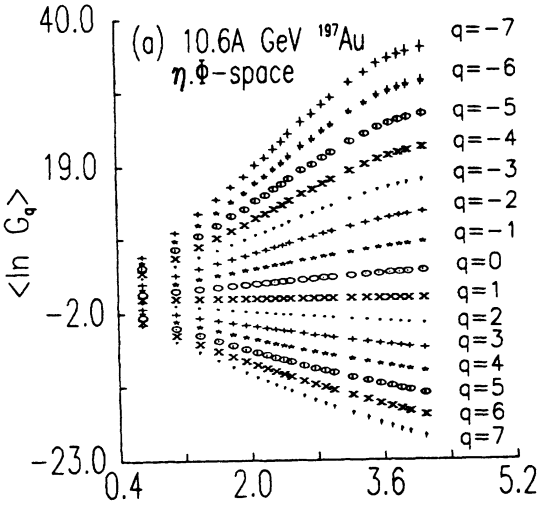

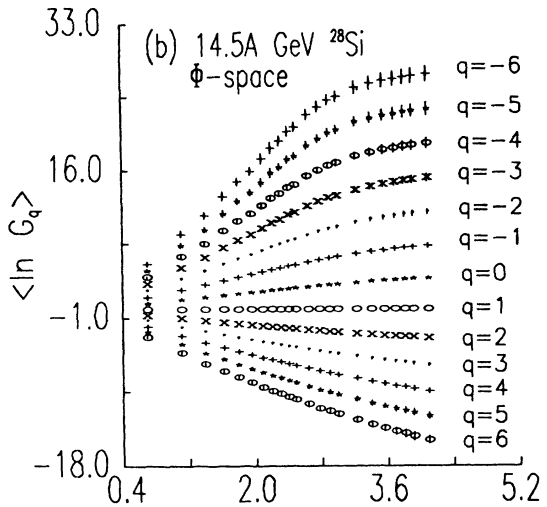

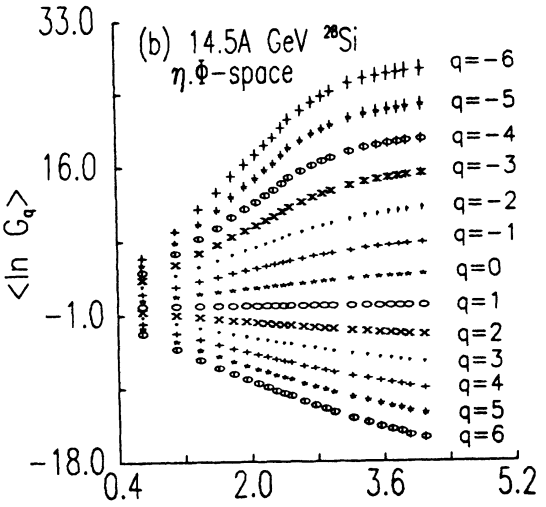

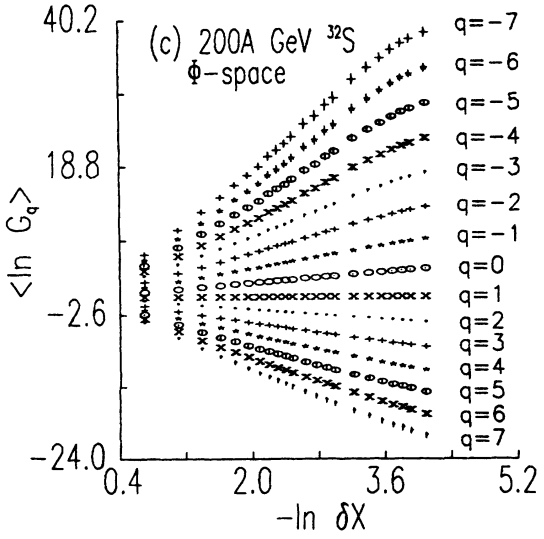

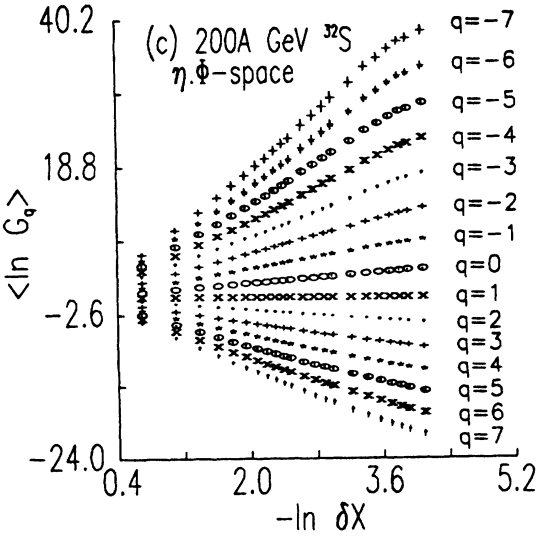

FIG. 3. The same as in Fig. 2, but in ϕ phase space.

FIG. 4. The same as in Fig. 2, but in η-ϕ phase space.

TABLE I. Values of slopes τ_q for ^{197}Au at 10.6A GeV, ^{28}Si at 14.5A GeV, and ^{32}S at 200A GeV projectiles in η phase space. Here, τ_q^{st} stands for the slopes of G_q moments for simulated events of these projectiles.

	Data samples			Simulated events		
	^{197}Au	^{28}Si	^{32}S	^{197}Au	^{28}Si	^{32}S
q	τ_q	τ_q	τ_q	τ_q^{st}	τ_q^{st}	τ_q^{st}
−7	−9.849±0.068	-	−10.059±0.093	−10.047	-	−9.795
−6	−8.843±0.055	−8.486±0.115	−8.650±0.075	−8.643	−8.728	−8.425
−5	−7.125±0.043	−7.127±0.091	−7.251±0.057	−7.248	−7.321	−7.069
−4	−5.783±0.032	−5.779±0.069	−5.872±0.038	−5.871	−5.925	−5.736
−3	−4.469±0.022	−4.455±0.049	−4.527±0.022	−4.528	−4.557	−4.443
−2	−3.312±0.014	−3.185±0.030	−3.245±0.009	−3.247	−3.246	−3.210
−1	−2.043±0.008	−2.009±0.016	−2.063±0.003	−2.061	−2.038	−2.061
0	−0.978±0.004	−0.955±0.007	−0.991±0.003	−0.984	−0.960	−0.997
2	0.913±0.006	0.870±0.009	0.931±0.003	0.917	0.870	0.948
3	1.780±0.013	1.682±0.019	1.818±0.008	1.785	1.678	1.859
4	2.614±0.021	2.456±0.031	2.672±0.014	2.618	2.445	2.742
5	3.426±0.029	3.203±0.043	3.503±0.021	3.425	3.186	3.602
6	4.221±0.038	3.933±0.055	4.232±0.027	4.214	3.909	4.445
7	5.005±0.047	-	5.119±0.035	4.990	-	5.275

TABLE II. Same as in Table I, but in ϕ phase space.

	Data samples			Simulated events		
	^{197}Au	^{28}Si	^{32}S	^{197}Au	^{28}Si	^{32}S
q	τ_q	τ_q	τ_q	τ_q^{st}	τ_q^{st}	τ_q^{st}
−7	−10.194±0.108	-	10.181±0.136	−10.000	-	−9.846
−6	−8.768±0.088	−8.749±0.119	−8.754±0.112	−8.605	−8.697	−8.468
−5	−7.351±0.068	−7.333±0.094	−7.338±0.086	−7.219	−7.296	−7.103
−4	−5.949±0.048	−5.929±0.070	−5.941±0.061	−5.850	−5.908	−5.762
−3	−4.579±0.030	−4.554±0.048	−4.579±0.036	−4.516	−4.548	−4.459
−2	−3.270±0.014	−3.239±0.029	−3.279±0.016	−3.241	−3.244	−3.219
−1	−2.063±0.006	−2.029±0.016	−2.080±0.004	−2.600	−2.040	−2.064
0	−0.981±0.004	−0.952±0.008	−0.995±0.001	−0.984	−0.962	−0.997
2	0.906±0.007	0.857±0.010	0.930±0.004	0.917	0.874	0.945
3	1.761±0.016	1.648±0.021	1.814±0.009	1.786	1.678	1.850
4	2.579±0.026	2.398±0.033	2.666±0.015	2.621	2.459	2.726
5	3.371±0.037	3.120±0.045	3.493±0.021	3.432	3.204	3.579
6	4.146±0.048	3.823±0.058	4.304±0.029	4.226	3.931	4.415
7	4.909±0.059	-	5.102±0.036	5.006	-	5.237

TABLE III. Same as in Table I, but in η-ϕ phase space.

	Data samples			Simulated events		
^{197}Au	^{28}Si	^{32}S	^{197}Au	^{28}Si	^{32}S	
q	τ_q	τ_q	τ_q	τ_q^{st}	τ_q^{st}	τ_q^{st}
−7	−10.478±0.095	-	−10.041±0.120	−10.076	-	−9.788
−6	−8.647±0.078	−8.655±0.114	−8.637±0.098	−8.667	−8.782	−8.420
−5	−7.254±0.060	−7.263±0.090	−7.244±0.075	−7.269	−7.359	−7.066
−4	−5.878±0.043	−5.882±0.067	−5.870±0.052	−5.887	−5.950	−5.735
−3	−4.533±0.027	−4.527±0.046	−4.532±0.031	−4.539	−4.570	−4.442
−2	−3.249±0.014	−3.227±0.027	−3.255±0.013	−3.253	−3.252	−3.210
−1	−2.059±0.007	−2.028±0.014	−2.072±0.003	−2.063	−2.040	−2.062
0	−0.981±0.004	−0.958±0.007	−0.994±0.001	−0.984	−0.961	−0.997
2	0.908±0.007	0.870±0.009	0.930±0.004	0.915	0.874	0.947
3	1.763±0.017	1.681±0.019	1.811±0.009	1.780	1.688	1.857
4	2.582±0.027	2.451±0.030	2.656±0.015	2.610	2.462	2.738
5	3.375±0.039	3.196±0.042	3.477±0.022	3.415	3.211	3.596
6	4.149±0.050	3.924±0.054	4.280±0.029	4.203	3.944	4.436
7	4.910±0.062	-	5.071±0.036	4.998	-	5.263

This shows that the dynamical fluctuations also exist in the multiplicity distribution of the produced hadrons in azimuthal ϕ phase space.

If a cascading mechanism is responsible for the production of jets of hadrons [16], then the dynamical fluctuations are expected to be more in higher dimensions. In order to explore the features of dynamical fluctuations in higher dimensions, we perform the multifractal analysis of our data in both of the variables η and ϕ simultaneously (η-ϕ phase space). The results of such an investigation are depicted in Figs. 4(a), 4(b), and 4(c) for projectiles A, B, and C, respectively. Just like in η or ϕ phase space, we once again observe a linear behavior of $\langle \ln G_q \rangle$ with $-\ln \delta X$, which is due to the dynamical fluctuations of the produced hadrons in η-ϕ phase space.

From Figs. 2, 3, and 4, the slopes τ_q are obtained by straight line fits through the linear portion of the data points for projectiles A, B, and C. In least-squares fitting for ions A and C, the last five data points were excluded, while for projectile B, the last seven points were ignored. The τ_q values along with their statistical errors as obtained from the above fittings are listed in Tables I, II, and III for η, ϕ, and η-ϕ variables, respectively, for the three ions used. From these tables, we may draw the following inferences: (i) The value of $d\tau_q/dq$ for negative values of q is always more than that for the positive q values in η, ϕ, and η-ϕ phase spaces. (ii) Although projectiles ^{197}Au and ^{32}S have quite different masses and energies, the values of τ_q, within errors bars, are very close to each other at every order of q in ϕ and η-ϕ phase spaces. However, in η-ϕ phase space for the values of $q \geq 2$, the τ_q values for the ^{32}S ion are more than that of the ^{28}Si ion. (iii) On a careful examination of the τ_q values for beams ^{197}Au, ^{28}Si, and ^{32}S in η, ϕ, and η-ϕ phase spaces indicate that for $q < -1$, τ_q values do not depend on the mass and energy of a given ion. However for $q \geq 0$, an apparent departure from this behavior is observed for the ^{28}Si data from ^{197}Au and ^{32}S data. (iv) In ϕ and η-ϕ phase spaces for $q \geq 0$, ^{28}Si data also depart from ^{197}Au and ^{32}S data. To study the effect of statistical contribution to G_q moments, a simple Monte Carlo simulation was performed. For each event with N particles, we distributed those particles randomly in the given interval ΔX to determine the statistical G_q and then averaged it over all the multiplicity distribution of a given real data sample. For every event, $\rho(X) = \text{const}$, and it implies a trivial dynamics due to a flat structureless X distribution for each event. The G_q moments for the simulated events also exhibited a power-law behavior characteristic of a self-similar system. For the simulated events of ^{197}Au, ^{28}Si, and ^{32}S beams in η, ϕ, and η-ϕ phase spaces, the slope values $\tau_q^{\rm st}$ are also presented in Tables I, II, and III. The deviation of τ_q from the statistical $\tau_q^{\rm st}$ is a measure of the real dynamics [5]. The implications of these results of simulated samples will be discussed in Fig. 6.

Derado *et al.* in Ref. [5] have presented a relationship to determine the dynamical value of the slope parameter $\tau_q^{\rm dyn}$ from the experimental τ_q and the statistical $\tau_q^{\rm st}$ components: $\tau_q^{\rm dyn} = \tau_q - \tau_q^{\rm st} + q - 1$. From this equation, for a particular data set given in Tables I, II, and III, the dynamical value of $\tau_q^{\rm dyn}$ can be obtained by inserting the value of τ_q and its corresponding statistical value $\tau_q^{\rm st}$ at any order of q. Thus, it is possible to compute dynamical values of the generalized dimensions $D_q^{\rm dyn}$ using Eq. (4). The $D_q^{\rm dyn}$ parameter is plotted in Figs. 5(a), 5(b), and 5(c) as a function of q in η, ϕ, and η-ϕ planes, respectively, for the ions A, B, and C. For all the projectiles A, B, and C, $D_q^{\rm dyn}$ is always positive for each order of q and $(0.9654 \leq D_q^{\rm dyn} \leq 1.0418)$ in η, ϕ, and η-ϕ phase spaces. For the ion C, $D_q^{\rm dyn}$ is always more than unity for $q \leq -1$ in η, ϕ, and η-ϕ phase spaces, which is contrary to the predictions of Ref. [5]. This inference is also valid for the ions A and B in ϕ phase space, when $q \leq -3$. For beam C in η, ϕ, and η-ϕ planes, $D_q^{\rm dyn}$ declines monotonically from a maximum to a minimum value as q is increased from -7 to 7, which is also true for the ions A and B in

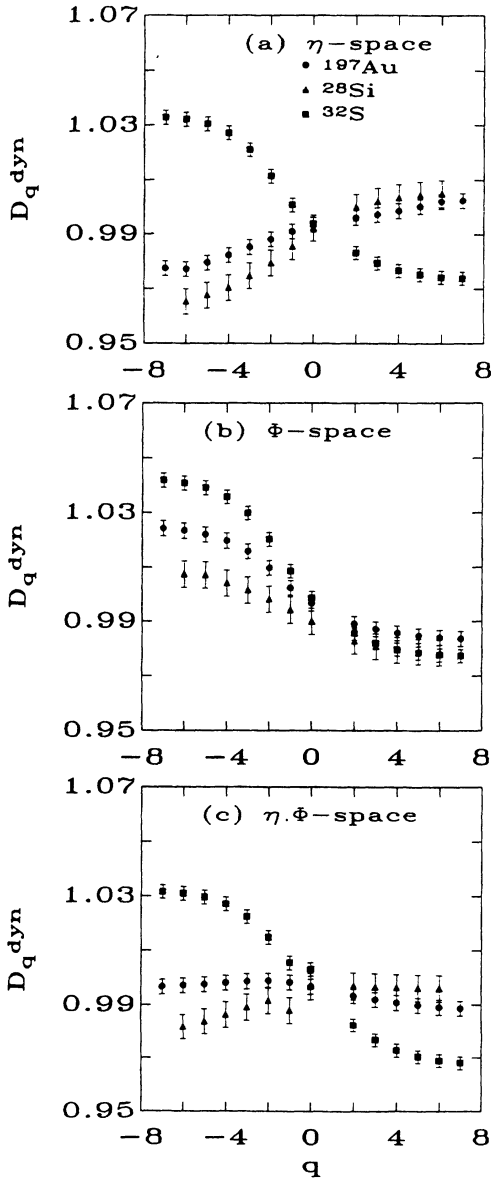

FIG. 5. $D_q^{\rm dyn}$ vs q for ions A, B, and C in (a) η, (b) ϕ, and (c) η-ϕ phase spaces.

ϕ phase space. However, for the projectiles A and B in η plane, $D_q^{\rm dyn}$ increases from a minimum to a maximum value, when q varies from -7 to 7. In η phase space, data obtained from BNL AGS (^{197}Au and ^{28}Si) overlap, within their statistical errors, for order $q \geq 0$, whereas a distinct separation between two data sets can be noticed for $q \leq -1$. ^{32}S data obtained from CERN has a quite distinctive behavior as compared to ^{197}Au and ^{28}Si data at all values of q. In ϕ phase space, within errors bars, all the data samples overlap for $q \geq 0$, while for $q \leq -1$ the three data sets diverge from each other. In η-ϕ phase space, ^{197}Au and ^{28}Si data samples, within the errors, have approximately the same values of $D_q^{\rm dyn}$ for $q \geq 0$, while for $q \leq -1$ the two data sets show an obvious departure from each other. The fractal $D_0^{\rm dyn}$, information $D_1^{\rm dyn}$, and correlation $D_2^{\rm dyn}$ dimensions for the three ions are given in Table IV, in η, ϕ, and η-ϕ phase spaces. Within error bars, the $D_0^{\rm dyn}$ and $D_1^{\rm dyn}$ dimensions seem to be independent of the mass and energy of a given ion in all the three phase spaces. The correlation ($D_2^{\rm dyn}$) dimension has the same magnitude for ^{197}Au and ^{28}Si beams in the η and η-ϕ phase spaces, while for the ^{32}S ion its magnitude is less than those for ^{197}Au and ^{28}Si. In the ϕ plane, the correlation dimension $D_2^{\rm dyn}$ has almost the same value for all three projectiles for $q > 0$. The terminal points of the curves in Figs. 5(a), 5(b), and 5(c) are all positive, indicating the absence of a phase transition according to the predictions of the Φ^3 model [17].

In Figs. 6(a), 6(b), and 6(c), we present a variation of $f(\Delta\alpha_q)$ as a function of the Lipschitz-Holder exponent α_q in η, ϕ, and η-ϕ phase spaces for all the ions used in this study. In these figures, $f(\Delta\alpha_q)$ represent the difference between the experimental and statistical values of $f(\alpha_q)$ for each data set used. In each case of Figs. 6(a) and 6(b), the multifractal spectrum $f(\Delta\alpha_q)$ is a continuous function of α_q, thus characterizing a qualitative manifestation of the dynamical fluctuations in the multiplicity distribution of a particular data set in η or in ϕ phase space. For $q > 1$, the $f(\Delta\alpha_q)$ spectrum represents a qualitative measure of the peaks, while for $q < 1$, it corresponds to the valleys in a given X distribution in either of the phase spaces for the individual events. The multifractal spectra depicted in Figs. 6(a), 6(b), and 6(c) satisfy a general feature of occurrence of a peak at α_0 and a common tangent at an angle of 45° at $\alpha_1 = f(\Delta\alpha_1)$. In η phase space, the $f(\Delta\alpha_q)$ spectra of ^{197}Au, ^{28}Si, and ^{32}S ions almost overlap for $q \leq 0$. However, for $q \geq 1$, the spectra of all the three beams diverge from each other. For the ^{197}Au and ^{28}Si projectiles in ϕ phase space, the $f(\Delta\alpha_a)$ spectra have almost the same width, but the ^{32}S ion spectrum has the least width in comparison to ^{197}Au and ^{28}Si spectra. The $f(\Delta\alpha_q)$ spectra of ^{197}Au and ^{28}Si ions in η-ϕ phase space are quite different from that of

TABLE IV. Values of generalized dimensions $D_q^{\rm dyn}$ for ^{197}Au at 10.6A GeV, ^{28}Si at 14.5A GeV, and ^{32}S at 200A GeV projectiles in η, ϕ, and η-ϕ phase spaces.

q	^{197}Au	^{28}Si	^{32}S
		η phase space	
0	0.9936±0.0027	0.9924±0.0048	0.9939±0.0025
1	0.9950±0.0027	0.9960±0.0048	0.9897±0.0024
2	0.9962±0.0027	1.0000±0.0048	0.9833±0.0027
		ϕ phase space	
0	0.9966±0.0027	0.9900±0.0048	0.9986±0.0025
1	0.9931±0.0027	0.9864±0.0047	0.9922±0.0024
2	0.9892±0.0027	1.9828±0.0047	0.9857±0.0024
		η-ϕ phase space	
0	0.9967±0.0027	0.9967±0.0048	1.0030±0.0025
1	0.9951±0.0027	0.9967±0.0048	0.9928±0.0024
2	0.9933±0.0027	1.9968±0.0048	0.9824±0.0024

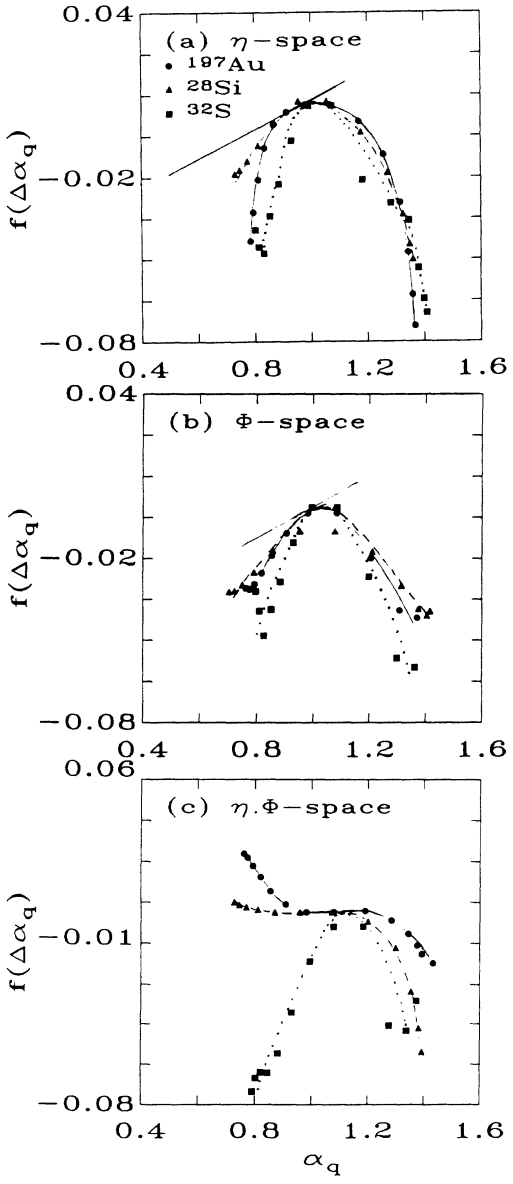

FIG. 6. Variation of $f(\Delta\alpha_q)$ vs α_q for projectiles A, B, and C in (a) η, (b) ϕ, and (c) η-ϕ phase spaces. Solid straight line represents a 45° line, tangent to $f(\Delta\alpha_q)$ at $\alpha_q = \alpha_1$. Free hand drawn curves are passed through three different data sets.

the ^{32}S ion, and, presently, we do not know the reason for this behavior of ^{197}Au and ^{28}Si ions.

V. CONCLUSIONS

The analysis of G_q moments has been performed by using a new scaled variable X suggested by Bialas and Gazdzicki [11]. Multifractal structures are revealed in the multiplicity distributions of shower particles produced in ^{197}Au-emulsion collisions at AGS energy. The results are compared with the available data on ^{28}Si and ^{32}S projectiles. The fractal properties seem to be an intrinsic characteristic prevailing in the dynamics of singly charged particles produced at relativistic energies. A downward concave shape of the multifractal spectral function $f(\Delta\alpha_q)$ indicates that the self-similar cascading mechanism [16] might be responsible for the production of final state particles in relativistic heavy ion collisions.

ACKNOWLEDGMENTS

We are thankful to the LBL technical staff for their help in the exposure and to Prof. G. Romano and Prof. Y. Takahashi for the development of emulsion stacks. This research work was supported by the Department of Energy through Grant No. DE-FG02-90ER40566.

[1] A. Bialas and R. Peschanski, Nucl. Phys. **B273**, 703 (1986); **B308**, 708 (1988).
[2] I.V. Ajinenko *et al.* (NA22 Collaboration), Phys. Lett. B **222**, 306 (1989); R. Holynski *et al.* (KLM Collaboration), Phys. Rev. Lett. **62**, 73 (1989); P.L. Jain and G. Singh, Z. Phys. C **53**, 355 (1992); Phys. Rev. C **44**, 854 (1991); M.I. Adamovich *et al.* (EMU01 Collaboration), Phys. Rev. Lett. **65**, 412 (1990); W. Kittel, in *Proceedings of the 20th International Symposium on Production Dynamics, Gut Holmecke, Germany, 1990*, edited by R. Baier and D. Wegner (World Scientific, Singapore, 1991), p. 401; Nucl. Phys. **B308**, 857 (1988).
[3] T. Viksec, *Fractal Growth Phenomenon* (World Scientific, Singapore, 1989); J. Feder, *Fractals* (World Scientific, Singapore, 1989).
[4] I.M. Dremin, Mod. Phys. Lett. A **3**, 1333 (1988); P. Lipa and B. Buschbeck, Phys. Lett. B **223**, 465 (1988); P. Carruthers, Int. J. Mod. Phys. A **4**, 5587 (1989); M. Blazek, Phys. Lett. B **247**, 576 (1990).
[5] R.C. Hwa, Phys. Rev. D **41**, 1456 (1990); C.B. Chiu and R.C. Hwa, *ibid.* **43**, 100 (1991); R.C. Hwa and J. Pan, *ibid.* **45**, 1476 (1992); I. Derado, R.C. Hwa, G. Jansco, and N. Schimtz, Phys. Lett. B **283**, 151 (1992).
[6] K. Sugano, Int. J. Mod. Phys. A **3**, 2249 (1988).
[7] G. Boca *et al.*, Nuovo Cimento **A105**, 865 (1992); C. Albajar *et al.*, Z. Phys. C **56**, 37 (1992).
[8] P.L. Jain, K. Sengupta, and G. Singh, Phys. Lett. B **241**, 273 (1990); P.L. Jain, G. Singh, and A. Mukhopadhyay, Phys. Rev. C **46**, 721 (1992).
[9] G. Singh, A. Mukhopadhyay, and P.L. Jain, Z. Phys. A **345**, 305 (1993).
[10] P.L. Jain, G. Singh, and A. Mukhopadhyay, Nucl. Phys **A561**, 651 (1993).
[11] A. Bialas and M. Gazdzicki, Phys. Lett. B **252**, 483 (1990).
[12] P.L. Jain, G. Singh, and A. Mukhopadhyay, Phys. Rev. C **48**, R517 (1993).
[13] G. Singh and P.L. Jain, Phys. Rev. C **49**, 3320 (1994).
[14] G. Singh and P.L. Jain, Z. Phys. A **4**, 99 (1994).
[15] P.L. Jain, K. Sengupta, and G. Singh, Phys. Rev. C **44**, 844 (1991).
[16] A. Bialas and R. Peschanski, Phys. Lett. B **207**, 59 (1988); W. Ochs and J. Wosiek, *ibid.* **214**, 617 (1988).
[17] R. Peschanski, Nucl. Phys. **B237**, 144 (1989).